Numerical Investigation of Mixed Convection incorporating Ag-H₂O Nanofluid inside Square Enclosure for Different Heater Locations

Anshuman Panigrahi[a], Bishwajit Sharma[b], Rabindra Nath Barman[c*]
Department of Mechanical Engineering
National Institute of Technology Durgapur
Mahatma Gandhi Avenue Marg, Durgapur, West Bengal, India
E-mails: [a]anshuman.panigrahi4@gmail.com,[b]sharmabishwajit93@gmail.com,[c]rn.barman@me.nitdgp.ac.in
Corresponding author

Abstract
The present study is an attempt to elucidate mixed convection flow in a shear driven enclosure incorporating silver nanofluid with a square cylindrical heat source placed at several locations. The simplicity from the point of view of computational expense has been achieved by carrying out 2-D simulations using the finite volume method. The effects of the change in heat source locations are studied observing the isotherms and average Nusselt number with respect to the concentration of silver in the nanofluid (0%, 1%, 3%, and 5%) and Richardson number (0.01, 0.1, 1 and 10) as decisive parameters. Prandtl number and Grashof number have been fixed to 6.2 and 10^4 respectively. The investigation is undertaken for five different locations of the square cylindrical heater. The study shows that maximum heat dissipation at higher Reynolds number occurs when the heater is placed near the bottom right corner of the enclosure; whereas in case of low Reynolds number, the heater when placed near the top left a corner of the enclosure yields maximum heat transfer. The investigation also yields a positive correlation between average Nusselt number with increasing silver concentration.

Keywords- Shear-driven flow, Silver nanofluids, Mixed convection, Finite volume method.

1. Introduction

Heat transfer is a fundamental phenomenon with a wide range of applications from nanofluids (Ahmad and Pop, 2010; Sharma et al., 2019; Ahuja, 2019) to prominent conventional energy sources like solar energy (Ideriah, 1980) and nuclear reactors (Guardo et al., 2006; Cha and Jaluria, 1984). Mixed convection in shear-driven enclosures is being extensively studied for its application in various experimental and industrial mechanisms and is being widely used for the validation of numerical solution procedures of Navier Stokes equation (Agarwal, 1981; Ghia et al., 1982; Morzynski and Popiel, 1988; Kaushik, 2019). Botella and Peyret (1998) used Chebyshev collocation method to accurately predict the flow within a standard shear driven enclosure at Reynolds Number of 1000 and henceforth established its validity. Koseff and Street (1984) studied the problem in a three-dimensional frame of reference and visualized the flow using the thymol blue technique and by rheoscopic liquid illuminated by laser-light sheets. Their research showed the significance of longitudinal Taylor-Görtler-like vortices and corner vortices in the end-wall regions in the flow regime.

Khanafer and Aithal (2013) studied the laminar flow inside a shear driven enclosure with a circular cylinder inside it using the Galerkin method of weighted residuals. The variation of average Nusselt number with Richardson number and the non-dimensional diameter of the cylinder showed that the Nusselt number increases with an increase in non-dimensional diameter when natural convection is dominant and reached saturation. But in the case of mixed convection, the Nusselt number

increases gradually without reaching a saturation point. Ovando-Chacon et al. (2013) analyzed the flow occurring inside a two-dimensional well-ventilated enclosure with a circular obstruction at the center. The various types of vortex formation mechanisms were identified and hence the study showed an improvement in the heat transfer capabilities of the enclosure with the addition of the circular obstruction. Tiwari and Das (2007) investigated the behaviour of nanofluids inside a differentially heated enclosure. Their results showed that the heat transfer profile of the flow was affected by both the direction of the moving walls and the Richardson number.

A study by Mehrizi et al. (2012) inspected the effect of nanoparticles on heat transfer in a well-ventilated enclosure with a hot obstacle. It was found that the addition of nanoparticles and an increase in their volume concentration enhances the heat transfer rate for various Richardson numbers. Based on these results, the present study incorporates silver nanofluid as the medium of flow as silver possesses higher thermal conductivity than water and its addition significantly improves the conductivity of the mixture. There are mainly two approaches to investigate the heat transfer phenomenon in media involving nanofluids; the first one is based on the two-phase model which incorporates the solid-fluid interaction within the fluid and helps to develop a better insight on the roles of both the media in heat transfer, the second and much simpler approach involves using a single-phase model in which both the media are considered to be in equilibrium and possess common local properties. The particle size of silver nanoparticles is less than 100 nm and the maximum concentration is less than 8%. Thus, the fluid is homogeneous and the molecular level motions and interactions can be neglected as the continuum is maintained (Khanafer et al., 2003). Hence a single-phase approach has been undertaken to carry out this investigation.

2. Mathematical Modelling
The square enclosure is having adiabatic lateral and bottom walls with the isothermal upper wall moving at a uniform velocity U_0. The flow inside the enclosure of side L is considered to be two-dimensional, steady, laminar and incompressible with a Grashoff Number of 10^4. A square cylindrical heat source of dimensions 0.25L X 0.25L is placed at various locations inside the enclosure as shown in Figure 1.
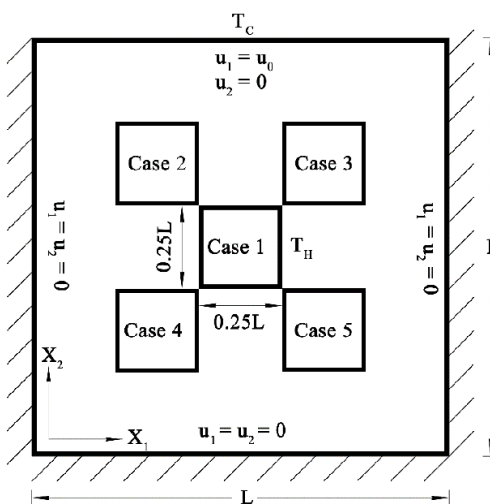

Figure 1. Schematic diagram of the enclosure with different positions of the heater

The isothermal heat source is denoted by a higher temperature T_H and the isothermal moving wall has a lower temperature T_C. The enclosure is filled with Ag-Nanofluid (Pr = 6.2) with its concentration (Ø) varying from 1% to 5% by volume. The properties of Water as a base fluid and Ag nanoparticles are enlisted in Table 1. The nanofluid has constant thermophysical properties throughout, except its density which varies based on the Boussinesq approximation. The nanofluid properties have been calculated based on the expressions used by Sharma et al. (2018) in his investigation of Cu-H_2O nanofluid.

Table1. Properties of water and silver nanoparticles

Basefluid		Silver (Ag)	
ρ_w	998.2	ρ_{Ag}	10490
$(C_p)_w$	4182	$(C_p)_{Ag}$	235
k_w	0.6	k_{Ag}	406

The effective density of Ag-nanofluid is

$$\rho_{nf} = (1-\phi)\rho_w + \phi\rho_{Ag} \tag{1}$$

and the heat capacitance of the Ag-nanofluid is given by

$$(\rho C_p)_{nf} = (1-\phi)(\rho C_p)_w + \phi(\rho C_p)_{Ag} \tag{2}$$

The effective thermal conductivity is calculated by the Maxwell-Garnett's approximation model. It is assumed that the nanofluid has spherical particle suspension.

$$\frac{k_{eff}}{k_w} = \frac{(k_{Ag} + 2k_w) - 2\phi(k_w - k_{Ag})}{(k_{Ag} + 2k_w) + \phi(k_w - k_{Ag})} \tag{3}$$

If n is the normal direction then the boundary conditions for different domains can be written as
For fluid domain:

$0 \leq X_1 \leq 1$	$X_2 = 0$	$U_1 = U_2 = 0$	$\frac{\partial \theta}{\partial n} = 0$
$0 \leq X_1 \leq 1$	$X_2 = 1$	$U_1 = 1, U_2 = 0$	$\theta = 0$
$X_1 = 0$	$0 \leq X_2 \leq 1$	$U_1 = U_2 = 0$	$\frac{\partial \theta}{\partial n} = 0$
$X_1 = 1$	$0 \leq X_2 \leq 1$	$U_1 = U_2 = 0$	$\frac{\partial \theta}{\partial n} = 0$

For Square cylindrical heater,

$$\theta = 1$$
(4)

The non-dimensional transport equations of mass, momentum, and energy for steady and incompressible flow are depicted in Eq. (1-4).

$$\frac{\partial U_1}{\partial X_1} + \frac{\partial U_2}{\partial X_2} = 0$$
(5)

$$U_1 \frac{\partial U_1}{\partial X_1} + U_2 \frac{\partial U_1}{\partial X_2} = -\frac{\partial P}{\partial X_1} + \frac{1}{\text{Re}}\left(\frac{\partial^2 U_1}{\partial X_1^2} + \frac{\partial^2 U_1}{\partial X_2^2}\right)$$
(6)

$$U_1 \frac{\partial U_2}{\partial X_1} + U_2 \frac{\partial U_2}{\partial X_2} = -\frac{\partial P}{\partial X_2} + \frac{1}{\text{Re}}\left(\frac{\partial^2 U_2}{\partial X_1^2} + \frac{\partial^2 U_2}{\partial X_2^2}\right) + Ri\theta$$
(7)

$$U_1 \frac{\partial \theta}{\partial X_1} + U_2 \frac{\partial \theta}{\partial X_2} = \frac{1}{\text{Re}\,\text{Pr}}\left(\frac{\partial^2 \theta}{\partial X_1^2} + \frac{\partial^2 \theta}{\partial X_2^2}\right)$$
(8)

For solid conducting square cylinder

$$\frac{\partial^2 \theta_s}{\partial X_1^2} + \frac{\partial^2 \theta_s}{\partial X_2^2} = 0$$
(9)

Where the dimensionless variables can be written as

$$X_1 = \frac{x}{L} \; ; \; X_2 = \frac{y}{L} \; ; \; U_1 = \frac{u_1}{U_0} \; ; \; U_2 = \frac{u_2}{U_0} \; ; \; \theta = \frac{(T - T_c)}{(T_h - T_c)} \; ; \; \theta_s = \frac{(T_s - T_c)}{(T_h - T_c)} \; ; \text{Re} = \frac{\rho U_0 L}{\mu} \; ; \; Ri = \frac{Gr}{\text{Re}^2} \; ; \; Gr = \frac{g\beta\Delta T L^3}{\upsilon^2}$$
$$; \text{Pr} = \frac{\mu C_p}{k} \cdot$$

The Nusselt number depends on the various thermophysical properties of the nanofluid like its volume fraction and thermal conductivity. For this particular problem, the average Nusselt number is computed according to Eq. (10)

$$\overline{Nu} = \frac{1}{L}\int_0^1 Nu.dX_1$$
(10)

3. Numerical Analysis and Validation
Finite Volume Method (FVM) is used to numerically solve the problem based on the commercially available solver Fluent. The pressure and momentum equations are coupled using the Semi-Implicit Method for Pressure-Linked Equation (SIMPLE) scheme, which has been deemed suitable for such kind of simple analysis by Patankar (1980). Quadratic Upstream Interpolation Convective Kinetics (QUICK) scheme is used to spatially discretize the convective terms of the problem. A convergence criterion of 10^{-13} was specified for both the energy and continuity equation for enhancing the accuracy of the analysis. A fine non-uniform mesh is generated with smaller cells near the wall boundaries as shown in Figure 2.

To validate the grid, domain with the first case was solved for Ri = 1 with Ø = 3 %. The average Nusselt number (Nu) was plotted for various grid sizes. The average Nu showed a significant variation for mesh count varying from coarse to a refined one with 20,984 nodes. Nu showed a fluctuation less than 0.005% beyond 20,984 nodes which can be accepted. Figure 3 represents the variation of Average Nu versus the number of nodes after computational study.
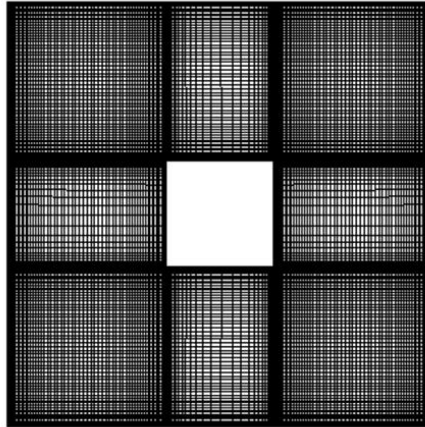

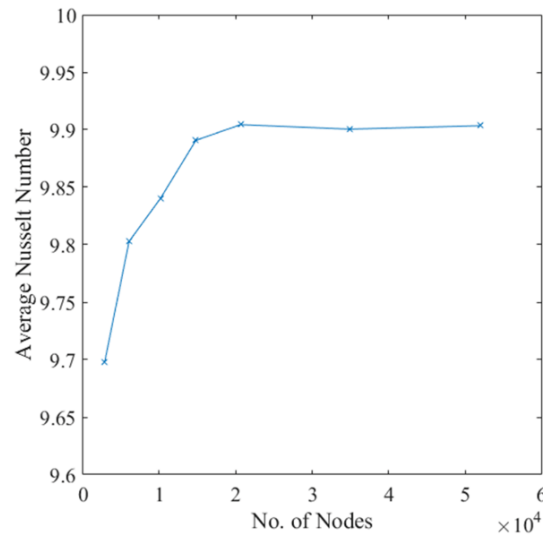Figure 2. Non-uniform and structured mesh for computational domain

Figure 3. The plot of average Nusselt number versus number of elements

The present numerical model is validated with the results of De Vahl Davis (1983) and Talebi et al. (2010) and the analysis showed satisfactory results with a good agreement which are shown in Figure 4.
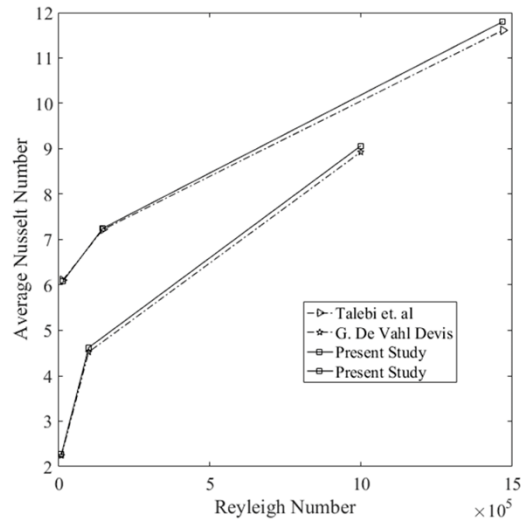

Figure 4. Scheme validation of the present study

4. Results and Discussions

The streamlines and isotherms of various Ag-nanofluid concentrations varying with the heater position are shown in Figure 5, Figure 6 (a, b) for $\emptyset = 0\%$, 1% and 3% respectively. The cases with low Richardson number (Ri) are governed by forced convection and the thermal profile drifts towards natural convection as the Ri increases to 10. Lid velocity bears a negative correlation with increasing Ri and causes a clockwise rotation in the flow field. The square cylinder heater acts as a mechanical blockage to the fluid flow but allows the heat transport by enhancing mixing inside the domain and hence resulting a better heat dissipation from the heater.

Figure 5 represents the isotherms and streamlines of the enclosure in the absence of nanoparticle. The square cylindrical heater, as a mechanical blockage, stimulates the formation of eddies which can trap heat, hence adversely affecting the thermal dissipation from the system. In Case 1, a central clockwise (CW) eddy is observed with two small counterclockwise (CCW) eddies in the bottom corners and a tiny eddy just above the heater. The heater lies at the centre of this eddy and hence heat is trapped within the eddy. This results in poor heat dissipation that can be seen in the isotherms of Case 1, which shows high isotherm concentration at the centre depicting poor heat transfer at low Reynolds number. Case 5, on the other hand, has an eddy just above the central heater, which substantially enhances the circulation of heat from the heater to the cold moving wall. This is illustrated by the isotherm which shows a rapid fall of temperature from the heater to the center of the eddy, rendering this location of the heater as the most efficient case for forced convection. This result is also supported by the plot of Nusselt number for Ri = 0.01 in Figure 7 which depicts that Case 5 has the highest Nusselt number. Case 2 depicts two large eddies; one on the right side of the heater (clockwise) and the other just below it (counterclockwise). The eddies in the other geometrical cases can be interpreted from Figure 5. The corresponding isotherms show the entrapment of heat in these eddies and the heat distribution across the profile. As the Richardson

number increases, the degree of forced convection slowly reduces and natural convection becomes dominant. It can be observed that upon increasing Ri, the streamlines slowly separate in Case 5 and break into two eddies, henceforth reducing its effectiveness for heat dissipation. The second eddy grows in size and gradually engulfs the heater as the Richardson number increases to 10, completely cutting it off from the eddy above it and hence resulting in extremely poor heat transfer, as can be concluded in Figure 7. It can also be observed that the eddy just in the right side of the heater in Case 2 starts circulating around the heater; pushing the hot fluid from the heater into the cold wall and enhancing heat circulation. This results in a sudden increase in the effectiveness of Case 2 for heat transfer as the Richardson Number increases from 0.1 to 10.

Figure 6 (a) and (b) shows the effect of heat transfer upon addition of nanoparticles to the base fluid. They show a similar trend in the isotherm and streamline profiles but the rate of heat transfer shows a substantial increase. Addition of nanoparticles increases the overall conductivity of the fluid and hence the net heat transfer increases.

Figure 7 shows the variation of average Nusselt number with nanofluid concentration (Ø) for the Richardson numbers 0.01, 0.1, 1 and 10 respectively. Based on the characteristics for Ri = 0.01 and 0.1, it is observed that Case 5 shows the best heat dissipation rate for forced convection. As the Richardson number increases and the heat transfer transforms from forced to natural convection, the geometrical configuration of Case 2 seems to show great improvement in its heat dissipation capability; having maximum heat transfer rates for the Richardson number of 1 and 10. The Nusselt number of Case 5 reduces to a minimum in case of natural convection due to the eddy on the left side of the heater that traps its heat, which fails to mix with the cold fluid resulting in extremely poor heat dissipation. The plot thus validates the conclusions made from the isotherm and streamline profiles of the enclosure depicted in Figure 5, 6 and 7.
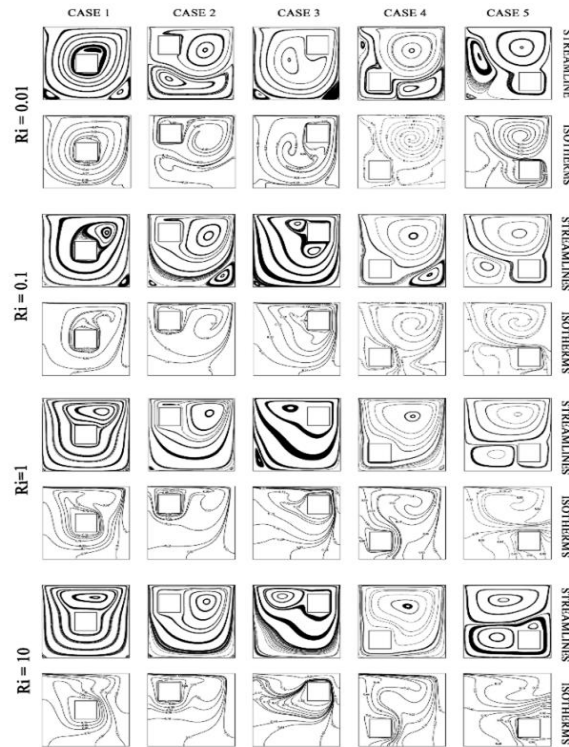
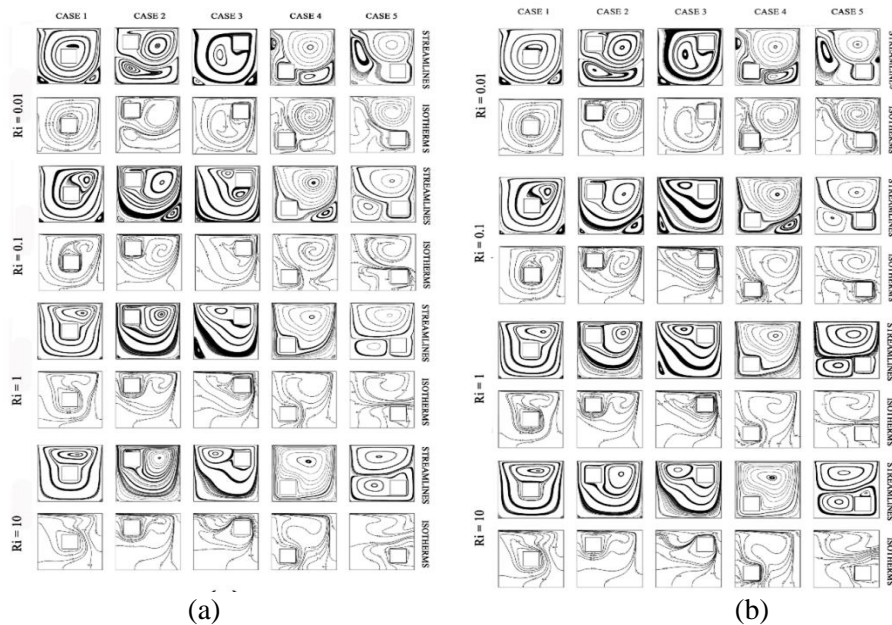Figure 5. Streamlines and isotherms for various geometrical cases at Ø = 0 %

(a)

(b)

Figure 6. Streamlines and isotherms for various geometrical cases (a) Ø = 1 % and (b) 3%
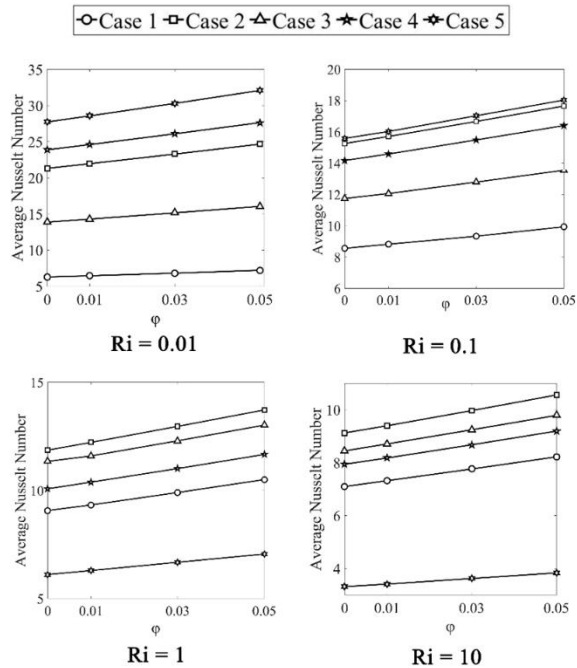
Figure 7. Characteristics of average Nusselt number versus Ø for Ri = 0.01, 0.2, 1 and 10

5. Conclusion

The aforementioned research builds up some concrete results regarding the heat dissipation rates and capabilities of various geometries at several Richardson numbers and nanofluid concentrations. Definitive correlations between their thermal and fluid profiles were obtained when subjected to natural and forced convection.

The best geometrical configuration for maximum heat transfer depends on the eddy formation based on the Richardson number; the heater when placed near the bottom right corner shows the best heat transfer for forced convection whereas natural convection is best suited for when the heater is placed near the top left corner. The Nusselt number characteristic of these cases also validate their thermophysical profiles as shown in the isotherm and streamline plots of the enclosure at different Richardson numbers and are well in synchronization with the heat-trapping and mixing capabilities of these eddies.

These observations find their applications in various industries from nanoscience to nuclear research. The manuscript provides the best geometric configurations for the placement of heat source in a shear driven enclosure; which can be implemented in heat exchangers and other heat transfer devices to substantially enhance their effectiveness. The observations also successfully validate the computational models used in this analysis, which provide results which are in sync with the actual physical phenomenon that the Nusselt Number shows a linear and positive correlation with the nanoparticle concentration.

Conflict of Interest

All authors have equal contribution in this work and declare that there is no conflict of interest for this publication.

References

Agarwal, R. (1981). A third-order-accurate upwind scheme for Navier-Stokes solutions at high Reynolds numbers. In *19th Aerospace Sciences Meeting* (p. 112). St. Louis, MO, U.S.A.

Ahmad, S., & Pop, I. (2010). Mixed convection boundary layer flow from a vertical flat plate embedded in a porous medium filled with nanofluids. *International Communications in Heat and Mass Transfer*, *37*(8), 987-991.

Ahuja, J., & Gupta, U. (2019). Rayleigh-Bénard convection for nanofluids for more realistic boundary conditions (rigid-free and rigid-rigid) using Darcy model. *International Journal of Mathematical, Engineering and Management Sciences, 4*(1), 139–156.

Botella, O., & Peyret, R. (1998). Benchmark spectral results on the lid-driven cavity flow. *Computers & Fluids*, *27*(4), 421-433.

Cha, C. K., & Jaluria, Y. (1984). Recirculating mixed convection flow for energy extraction. *International Journal of Heat and Mass Transfer*, *27*(10), 1801-1812.

De Vahl Davis, G. (1983). Natural convection of air in a square cavity: a benchmark numerical solution. *International Journal for Numerical Methods in Fluids*, *3*(3), 249-264.

Ghia, U. K. N. G., Ghia, K. N., & Shin, C. T. (1982). High-Re solutions for incompressible flow using the Navier-Stokes equations and a multigrid method. *Journal of Computational Physics*, *48*(3), 387-411.

Guardo, A., Coussirat, M., Recasens, F., Larrayoz, M. A., & Escaler, X. (2006). CFD study on particle-to-fluid heat transfer in fixed bed reactors: Convective heat transfer at low and high pressure. *Chemical Engineering Science*, *61*(13), 4341-4353.

Ideriah, F. J. K. (1980). Prediction of turbulent cavity flow driven by buoyancy and shear. *Journal of Mechanical Engineering Science*, *22*(6), 287-295.

Kaushik, A. (2019). Numerical study of 2D incompressible flow in a rectangular domain using Chorin's projection method at high Reynolds number. *International Journal of Mathematical, Engineering and Management Sciences, 4*(1), 157–169.

Koseff, J. R., & Street, R. L. (1984). The lid-driven cavity flow: a synthesis of qualitative and quantitative observations. *Journal of Fluids Engineering*, *106*(4), 390-398.

Khanafer, K., & Aithal, S. M. (2013). Laminar mixed convection flow and heat transfer characteristics in a lid-driven cavity with a circular cylinder. *International Journal of Heat and Mass Transfer*, *66*, 200-209.

Khanafer, K., Vafai, K., & Lightstone, M. (2003). Buoyancy-driven heat transfer enhancement in a two-dimensional enclosure utilizing nanofluids. *International Journal of Heat and Mass Transfer*, *46*(19), 3639-3653.

Mehrizi, A. A., Farhadi, M., Afroozi, H. H., Sedighi, K., & Darz, A. R. (2012). Mixed convection heat transfer in a ventilated cavity with hot obstacle: effect of nanofluid and outlet port location. *International Communications in Heat and Mass Transfer*, *39*(7), 1000-1008.

Morzynski, M., & Popiel, C. O. (1988). Laminar heat transfer in a two-dimensional cavity covered by a moving wall. *Numerical Heat Transfer*, *13*(2), 265-273.

Ovando-Chacon, G. E., Ovando-Chacon, S. L., Prince-Avelino, J. C., & Romo-Medina, M. A. (2013). Numerical study of the heater length effect on the heating of a solid circular obstruction centred in an open cavity. *European Journal of Mechanics-B/Fluids*, *42*, 176-185.

Patankar, S. V. (1980). *Numerical heat transfer and fluid flow*. CRC press New York. ISBN: 978-0-89116-522-4

Sharma, B., Kumar, B., & Barman, R. N. (2018). Numerical investigation of Cu-water nanofluid in a differentially heated square cavity with conducting solid square cylinder at centre. *International Journal of Heat and Technology*, *36*(2), 714-722.

Sharma, J., Gupta, U., & Shukla, S. (2019). A revised model for magneto convection in binary nanofluids. *International Journal of Mathematical, Engineering and Management Sciences, 4*(1), 131–138.

Talebi, F., Mahmoudi, A. H., & Shahi, M. (2010). Numerical study of mixed convection flows in a square lid-driven cavity utilizing nanofluid. *International Communications in Heat and Mass Transfer*, *37*(1), 79-90.

Tiwari, R. K., & Das, M. K. (2007). Heat transfer augmentation in a two-sided lid-driven differentially heated square cavity utilizing nanofluids. *International Journal of Heat and Mass Transfer*, *50*(9-10), 2002-2018.